Geological storage of CO_2: Heterogeneity impact on pressure behavior

Meisam Ashraf

November 23, 2013

Abstract

Due to the high rates of industrial CO_2 emission, it is an operational objective to maximize CO_2 injection rates into underground geological formations. Forcing high volumetric rates into the injection wells can result in an over-pressurized system, which can cause possible breaches in the formation integrity and can increase the risk of CO_2 leakage.

The goal of this study is to investigate and control the pressure buildup during injection to avoid the uncontrolled development of fractures in the medium. Herein, we study how geological heterogeneity influences the pressure behavior of a typical CO_2 injection operation. Five geological feature variables are considered as inputs for the sensitivity analysis. These features include various degrees of faults, lobosity, flow barriers, aggradation angle, and progradation direction.

Two injection scenarios are examined. In the first scenario, CO_2 is injected through a single well at a constant rate and the pressure in the well and the domain is allowed to build up without limit. In the second scenario, a pressure constraint is set on the well and the target injection rate is reduced to keep the pressure below the safety limit. Model responses related to pressure buildup and propagation within the system are defined and demonstrated using a single geological realization. Results for all realizations are presented and discussed accordingly. We conclude by ranking aggradation angle, progradation direction, and faults as the most influential geological parameters.

The novelty of this work lies in the use of a large parametrized ensemble of equiprobable and realistic geological realizations to analyze how pressure builds up and propagates through the storage medium. The demonstrated workflow is generic and can be used in any extensive pressure study. Likewise, our investigation reveals several generic patterns in how the different geological parameters influence the pressure buildup in this type of shallow-marine systems, but the relative ranking of which parameters are the most important may, of course, change if one selects a different injection scenario, injection location, number of injector, or set of geological realizations.

1 Introduction

The industrial CO_2 emission rate is expected to increase over the next decade if necessary preventive actions are not taken. For example, according to the Energy Information Administration, carbon dioxide emissions in the United States are forecast to reach 6.41 billion tonnes by 2030. The Kyoto Protocol proposed an emission cut that requires a reduction of 1.75 billion tonnes of carbon dioxide [16].

Geological storage of CO_2 is a proposed solution to fight global climate change. Clear operational criteria and policies must be put forward to avert unwanted consequences. Concerns connected to putting large volumes of CO_2 into underground geological formations are not limited to the spatial distribution of the injected fluid. The pressure signals imposed through the injection point can travel beyond the scale of the zones where CO_2 is present. Although geological barriers can hinder the pressure exchange between different regions, pressure can transfer through low-permeable rocks where the CO_2 is trapped by capillarity.

In addition to the depleted oil and gas fields, deep geological aquifers are practical targets for the geological storage of CO_2. If one is injecting into brine aquifers, the pressure waves can push the brine into connected fresh water aquifers, contaminating them. Brine displacement issues are discussed in [5] by defining open, closed, and semi-closed aquifer boundaries. Brine might also leak through abandoned wells into other zones. Cailly et al. [4] discuss how to design the injection process to prevent any leakage through wells.

Geomechanical deformations are important during the injection period. They can lead to changes in effective permeability and porosity. It is possible that the pressure buildup around injection wells can crack the rock with uncontrolled fractures extending to the structural sealing layers. Faults can be activated due to high pressure in the system, providing a leakage path across layers. In addition to the increased spatial spread of CO_2, an intensive induced fracture network can result in local earthquakes.

Simplified geological assumptions allow the use of established analytical solution of the flow governing equations. Neuman and Witherspoon [11] presented solutions that are useful for determining the hydraulic properties of leaky confined aquifer systems. They assumed that the aquifer is homogeneous, isotropic, and of uniform thickness. Moreover, they assumed the spatial extent of the aquifer to be infinite. Chabora and Benson [6] used the analytical solution provided in [11] to study the leakage of the stored CO_2 through the caprock by measuring the pressure buildup in the aquifer. They performed sensitivity analysis on the pressure variation by changing the formation parameters and injection criteria. Chabora and Benson found a correlation between the pressure buildup values in the medium and the specifications of aquifer and injection operations. This correlation gives insight in the design and monitoring phases of the storage operations. Such pressure monitoring approaches are based on geological simplifications.

Injection causes pressure evolution in the domain that starts by transient pressure buildup near the injector. As the injection proceeds, the injected CO_2 invades larger region in the domain. The two-phase region grows in size and the injected CO_2 moves in both vertical and horizontal directions within the aquifer. In the vertical direction, the CO_2 moves upward due to the buoyancy forces and in the horizontal direction the influx from the injector pushes the CO_2 through the two-phase zone. When the pressure pulse imposed by the injector reaches the boundaries of the domain, the average pressure in the aquifer increases in a

quasi-steady state trend. Pressure buildup development in the medium, in particular the transient pressure changes, can be influenced dramatically by geological heterogeneities. This study aims to evaluate the importance of sophisticated geological modeling in simulating the pressure variation in the domain.

Spatial pressure distribution in the aquifer depends on the extent of the domain. The available volume for CO_2 storage in closed or semi-closed systems with limited spatial extent is mostly provided by medium compressibility in response to formation pressure buildup. Moreover, the caprock and structural traps that are supposed to be sealing may allow the CO_2 to leak at a rate that depends on the pressure buildup in the aquifer. Birkholzer et al. [3] investigated the influence of domain size on pressure rise in the medium caused by CO_2 injection, assuming a homogeneous aquifer to study the pressure development for various model sizes, ranging from 10 to 100 km. They simulated CO_2 injection over 30 years in 250 m thick formation with a rate of 120 kg/s, and performed sensitivity analysis with focus on the plume migration and the evolution of pressure buildup in the aquifer. In addition to the spatial extent, various hydrological properties were examined to study the impact on CO_2 storage capacity. The results in [3] suggest that the storage capacity in closed and semi-closed aquifers is controlled by the operational pressure constraints and it is much smaller than the capacity of large aquifers. The simulations in [3] show that the region of elevated pressure is much larger than the size of the CO_2 plume. In a 20 km model, a substantial pressure increase of 45 bar from hydrostatic was observed at the model boundaries. They used closed boundary condition in the model that caused a global pressurizing in the medium. A local pressure rise above 60 bar was simulated near the injection well.

In general, constraints must be imposed on the bottom-hole pressure of the injection well to limit the pressure buildup in the aquifer, which will typically reduce the injection rate that is possible to safely achieve. Rock quality within the injection region has a significant impact on pressure buildup and therefore geological uncertainty plays a considerable role in assessing the success and feasibility of the operation. Most of the pressure-related studies in the literature provide either deterministic case studies or generic preventive measures based on theoretical studies [12, 17, 8, 18, 14, 13]. It is important to include realistic geological descriptions in any geological uncertainty study. For example, realistic permeability variation in the grid should be included, possibly in the form of an ensemble of equiprobable realizations.

Within the context of oil recovery, the impact of geological uncertainty on different field-development strategies is thoroughly investigated in the SAIGUP project for shallow-marine depositional systems [7, 9, 10]. Based on several injection/production patterns, the study concludes that geological uncertainty has a dramatic influence on the oil recovery estimates. We have previously used a number of geological realizations from the SAIGUP project to investigate the impact of geological uncertainty on the injection and early migration of CO_2 [2, 1]. The focus in these studies was to use the parametrized ensemble of geological realizations to measure how sensitive the spatial CO_2 distribution is to variations in the geology. Certain structural features were considered and several flow responses were defined to measure the storage capacity, the trapping efficiency, and the leakage risk. The sensitivity of these responses to variations in geological parameters was investigated. The results show that varying the geology gives large variation in responses, and aggradation angle and barrier coverage were found to have the most significant impact on the CO_2 flow behavior [2, 1].

Herein, we will use the same SAIGUP geological realizations to perform detailed analysis of how geological variations impact the pressure buildup and propagation in aquifers. The spatial extent of the SAIGUP models, 9 km × 3 km ×80 m, is considerably smaller than the extent of large aquifers. To compensate for the size, we consider open boundary conditions by exaggerating the pore volume of the cells at the boundaries of the model. This choice of boundary modeling results in an early relaxation of the pressure in the medium when the pressure pulse arrives at the boundary. Overall, the pressure values reported in our study can therefore be expected to be higher if they were modeled in a larger model. This study complements [2, 1], in the sense that we herein analyze the sensitivity of pressure to the same geological parameters. In addition to the injection scenario used in [2, 1], we examine a different injection scenario with more realistic well control for the injection operation. Our study shows that details in the geology can have a pronounced effect on the pressure development, which demonstrates the importance of realistic and detailed geological modeling when designing CO_2 storage operations and monitoring the pressure development in the aquifer. To the best of our knowledge, this is the first pressure study in the context of CO_2 storage that considers the geological uncertainty in the form of a parametrized set of structural and sedimentological variables.

2 Geological parameters

In the SAIGUP study, six rock types were included to model a shallow-marine system. Each rock type was modeled at appropriate scales to honor the interaction of flow with various heterogeneity types at different spatial scales (Figure 1). Each facies was upscaled in a number of stages and finally all the rock types were mapped on a fine-grid geological model. Some of the meter-scale facies were modeled in three dimensions to capture anisotropy. Variation within each rock type was modeled either deterministically by considering a periodic pattern or modeled internally by stochastic population. Channels were modeled on the fine grid and went through two stages of upscaling. Tests showed that when upscaled, models with different grid resolutions produced similar results. The specifications of the rock types are given in Table 1. For more detail of the SAIGUP sedimentological modeling see [7].

Table 1: The facies used in the SAIGUP geological modeling and their modeling scales.

Facies name	**X Scale**	**Y Scale**	**Z Scale**
Offshore transition zone	0.5 m	0.5 m	0.5 cm
Lower shoreface	0.5 m	0.5 m	0.5–2.0 cm
Upper shoreface	0.5 m	0.5 m	0.2–0.5 cm
Coastal plane	75 m	—	—
Offshore	75 m	—	—
Channels	0.04–1 m	0.04–1 m	0.5 cm

The wave and fluvial depositional processes acting at the shoreline control the plan-view shape, the channel abundance in the delta plain, and the abundance of mud-drapes. These parameters were characterized and summarized as three different types of shorefaces. A wave-dominated deposition produces a straight plan-view shape, very few channels, and no dipping

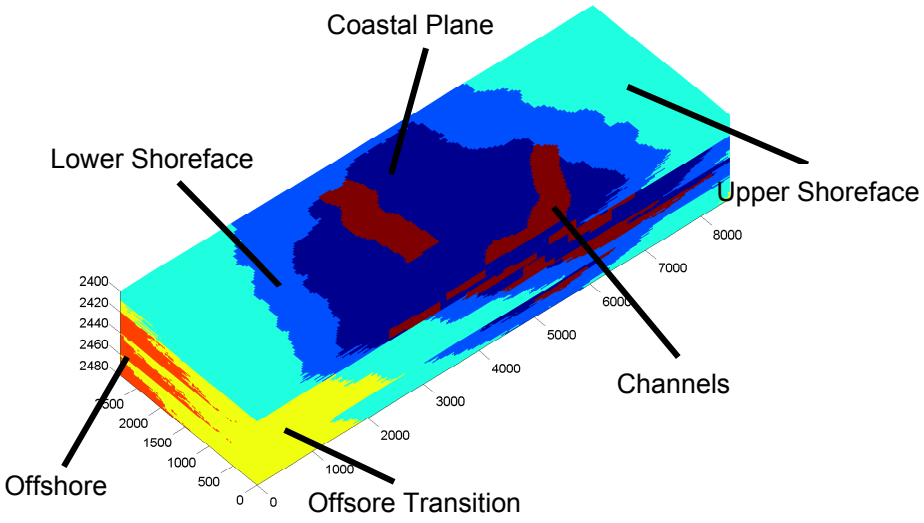

Figure 1: Geological modeling in the SAIGUP realizations contains six facies that represent a shallow-marine system. The rock types are represented by various colors for a selected realization. Axes show the spatial dimention of the model in meter.

Table 2: Specification of geological and simulation models; averaged values are arithmetic averages and belong to the specific geological realization shown in Figure 1.

Parameter	**Value**
Model dimensions	3 km×9 km×80 m
Geological grid resolution	$80 \times 240 \times 80$
Simulation grid resolution	$40 \times 120 \times 20$
Simulation grid resolution	$40 \times 120 \times 20$
Average of lateral permeability	181 mD
Average of Vertical permeability	26.8 mD
Average of porosity	0.145

Table 3: Colors and line and marker types used to signify different values of the geological parameters outlined in Figure 2.

Code	Description	Color/line/marker	Feature values
Thickness	Fault	thin/medium/thick	unfaulted/open/close
Shape	Lobosity	square/circle/diamond	flat/one-lobe/two-lobe
Size	Barriers	small/medium/large	10% / 50% / 90%
Color	Aggradation	blue/green/red	low/medium/high
Case no. counting	Progradation	first half/second half	up-dip / down-dip

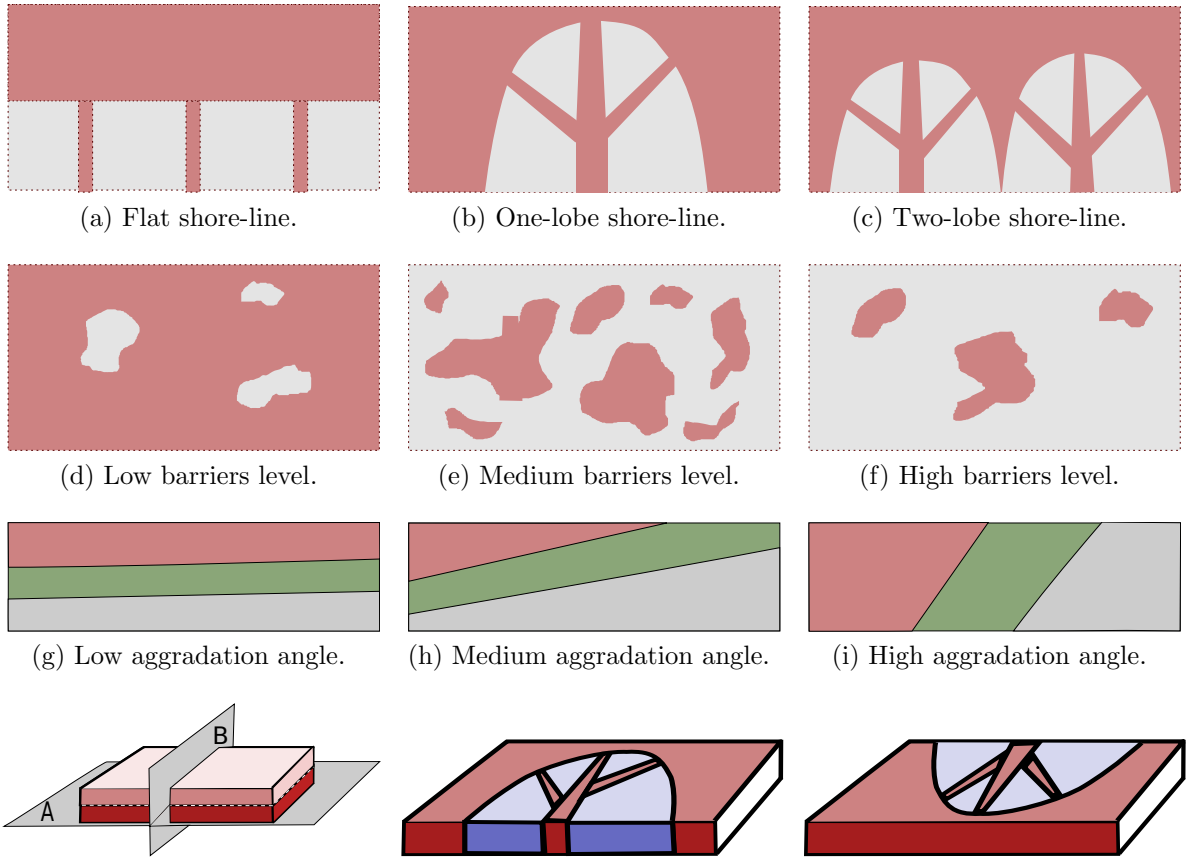

(a) Flat shore-line. (b) One-lobe shore-line. (c) Two-lobe shore-line.

(d) Low barriers level. (e) Medium barriers level. (f) High barriers level.

(g) Low aggradation angle. (h) Medium aggradation angle. (i) High aggradation angle.

(j) Slice A is used in Figures a–f and B in Figures g–i. (k) Up-dip progradation. (l) Down-dip progradation.

Figure 2: The studied geological features. a–c) Shoreline shape, gray is for poor quality rock and brown color resembles a good quality rock. d–f) Barriers level defined by transmissibility multiplier; gray color is for zero and brown color shows one. g–i) Aggradation angle. k–l) Progradation direction. Figure j shows the slices used in other figures.

barriers. If the river flux is high enough to dominate the wave system in the sea, a lobate shape shoreface generates with a moderate number of channels and some dipping barriers. Higher levels of fluvial domination end up in two-lobe system with numerous channeling and dip barrier surfaces.

Shale-draped surfaces may provide both horizontal and vertical barriers to fluid flow and are common in fluvial-dominated systems. They are the product of very short-term fluctuations in the fluvial systems and periodic floods in the delta. Shore line shape is correlated to the shape of these flow barriers; straight shorelines typically have planar seaward-dipping clinoforms and curved shorelines have clinoforms that resemble top-truncated cones. Within SAIGUP, these barrier surfaces were modeled as stepped transmissibility multipliers on the cell faces. Dipping barriers were not included in the flat shoreline models and in the realizations with lobosity, between one and three barriers were included. For the purpose of SAIGUP, three levels of barrier coverage were modeled for all of the SAIGUP models (10%, 50% and 90% coverage). All levels of coverage were subsequently slightly modified by removing the barriers where the fluvial channel deposits were present, since clinoforms are a feature of the delta front and not formed within a channel setting.

Aggradation angle models the variation of shoreline in a 2D depositional dip-orientated cross-section. Within SAIGUP, the trajectory varies between horizontal progradation and pure vertical aggradation. Aggradation angle is a function of the balance between sediment supply and the rate of accommodation in the sea. When the fluvial flux increases in level, the deposition from the river toward the sea pile toward the sea and makes the aggradation angle.

The final factor varied during the sedimentological modeling was the progradation or depositional-dip direction. Figure 2 shows a schematic of each geological parameter with its variation. The progradation direction is important for CO_2 injection operations because the structural dip controls the injection well position and the direction of CO_2 plume movement during injection. In Figure 3, injecting in high permeability channels enhances the well injectivity and lowers the pressure buildup in the medium.

The faults are modeled as post-depositional with no related changes in facies thickness or shoreline orientations. Faulting process causes layers with different quality to become adjacent (Figure 4). This can enhance the pressure connectivity by breaking sealing layers, or it can produce sealed compartments that are not connected to the rest of the domain.

In the last step of the SAIGUP modeling process, the geological realizations were upscaled via flow-based methods to a coarse grid that was found suitable for detailed flow simulations. Details of geological and simulation grids are given in Table 2.

Herein, we have selected four of the geological parameters from the SAIGUP project (Figure 2) to study the impact of heterogeneity in the petrophysical parameters on the pressure responses in a typical CO_2 injection problem. Altogether, this gives 54 different petrophysical realizations. In addition, we consider three different degrees of faulting in the models: unfaulted, open, and closed faults (Figure 5). Combining all the features and levels makes 162 cases. However, two cases were missing in the original data set and in the following we will therefore consider 160 different models. Each of these models are represented with different colors, line types, and marker types and sizes, as explained in Table 3.

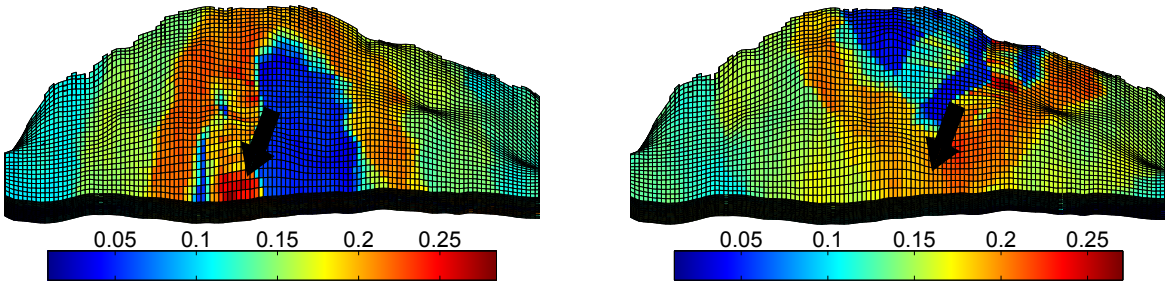

(a) Up-dip progradation.

(b) Down-dip progration.

Figure 3: Progradation dip direction shown by porosity for a case with one lobe. Arrows point to injection locations in the flank. Up-dip proragdation (left) contains heterogenities in the form of high contrast channels surronded by poor quality rocks. The injectivity in this case can be dramatically good or bad, depending on the well location. On the other hand, down-dip progradation (right) provides a lower contrast in the flank that can be low rock quality in general with low injection quality.

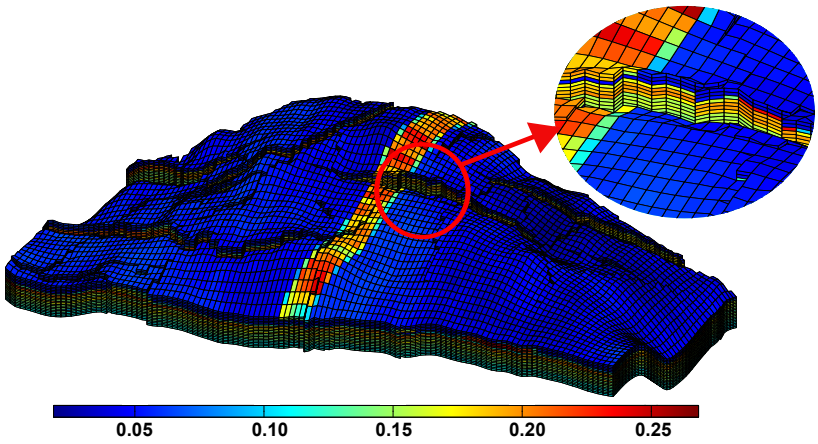

Figure 4: Faults connect layers with different rock types. Porosity is shown ion the grid. Across the fault, layers with low pore volume and permeability (the latter is not shown here) sit next to high pore volume and permeability layers.

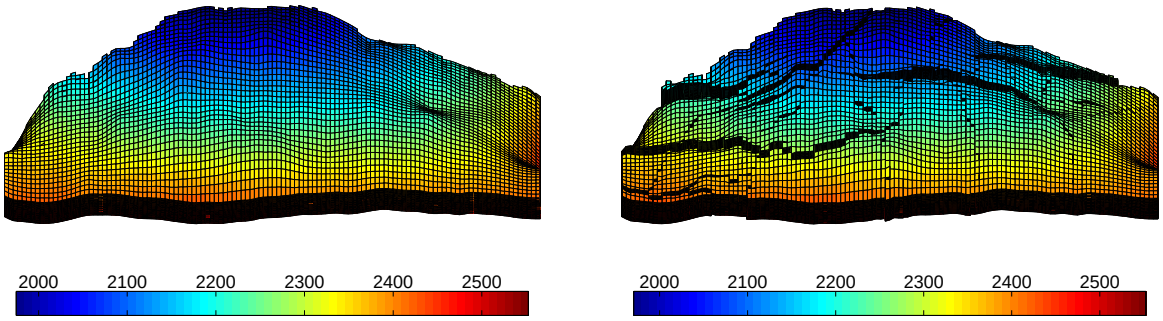

(a) Unfaulted grid. (b) Faulted grid.

Figure 5: Structural models used in the study. Depth in meter is shown by color. In the faulted structure, faults exist both in the dip and lateral directions.

3 Injection scenario

We assume open boundaries on the sides of the simulation model (Figure 6). The spatial dimensions of the model are relatively small (9km×3km×80m). Therefore, assuming closed or semi-closed boundaries results in an unrealistic pressure buildup in the domain due to the injection operation. The open boundaries are modeled by exaggerating the two last cells at the boundaries. The second last cell pore volume is magnified 10^3 times and the pore volume of cells at the boundary is multiplied by 10^6. These values are calculated such that no considerable pressure change occurs in the out-most cells at the boundary. No-flow boundary condition is applied on the top and bottom of the model. Moreover, the evaluated side on the crest is located at a large fault displacement and is considered as a close boundary.

The study will be limited to a single injection point so that we can study how the medium responds to the pressure imposed by a vertical injection well, whose position and completions are assumed to be fixed across all realizations. The position and completions were decided by studying a homogeneous model. One big plume will form around the injection point and migrate upward in the domain because of buoyancy forces. To maximize the potential for structural and residual trapping as the plume migrates in the up-dip direction toward the crest of the model, we chose an injection point down in the flank, some distance away from the lower boundary to reduce the possibility of fluids being pushed out through this boundary in the down-dip direction. The well was completed in the four deepest cells corresponding to the lowest layer of the model. Completing the well in the same four cells for all realizations may exaggerate pressure buildup if the well is completed in a low-permeable region, but has the advantage that we keep the comparison between the different realizations as simple as possible and avoid introducing extra parameters in the study. In a real storage operation, one would likely seek to optimize the injection point and complete the well in geological layers that have a satisfactory injectivity. In a more comprehensive study, one should therefore perform simulations for multiple injection locations, but as this would dramatically increase

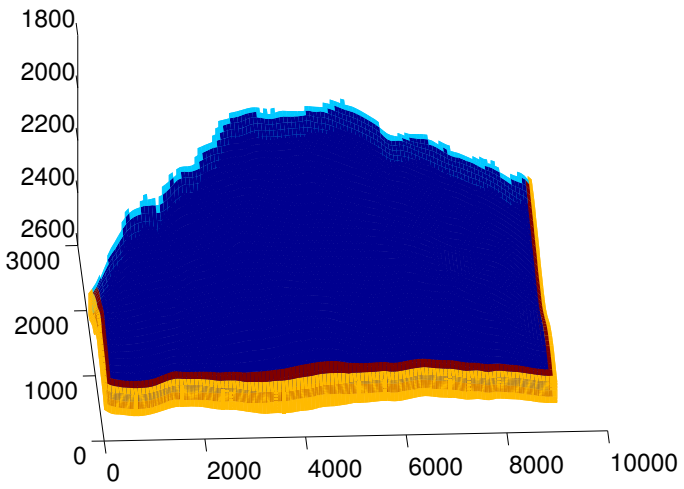

Figure 6: Boundaries in the flow simulation model; the crest boundary (light blue) is considered closed to flow. The pore volume of the cells at the other sides of the model are multiplied by 10^3 (red) and 10^6 (yellow) to model open boundaries.

the required number of detailed flow simulations, such simulations are not conducted in this study.

Instead, we will consider two strategies for injecting a volume of 4×10^7 m^3 of supercritical CO_2, which amounts to 20% of the total pore volume of the models. In the first strategy, which is similar to the one used in [2], the entire CO_2 volume is injected within 30 years using a constant volumetric rate. In the second strategy, the injector operates with the priority of injecting a volumetric rate of 3650 m^3/day. A pressure constraint of 400 bar is set on the injector. If the well bottom-hole pressure goes higher than that, the well priority changes to continue operating at 400 bar by reducing the injection rate until the target CO_2 volume is injected into the medium. As soon as the total injected volume reaches total target, the injector is shut in from the bore-hole and no injection happens for the rest of simulation time up to 100 years.

A standard simulator for multiphase flow in porous medium is used that is based on finite volume method [15]. Two phases (water and supercritical CO_2) are considered with no mass exchange between them. The fluid compressibility C_{fluid} is used to model the phase density changes with pressure variation from reference pressure P_0:

$$\rho = \rho_0 + C_{fluid}\rho_0(P - P_0).$$

Effect of rock compressibility is considered by C_{rock}:

$$C_{rock} = \frac{\partial \phi}{\partial P}.$$

The water and supercritical CO_2 are assumed to be slightly compressible, with fluid parameters described in Table 4.

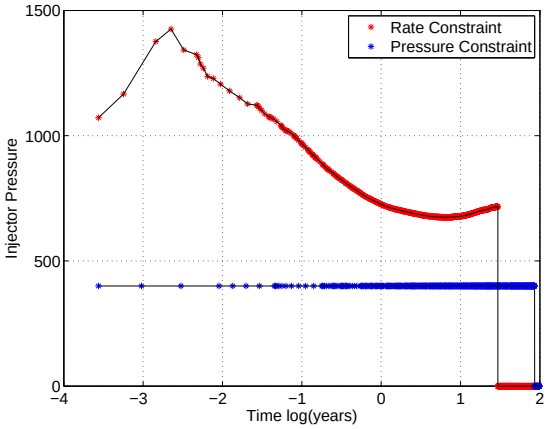

(a) Pressure in the injector versus logarithm of time.

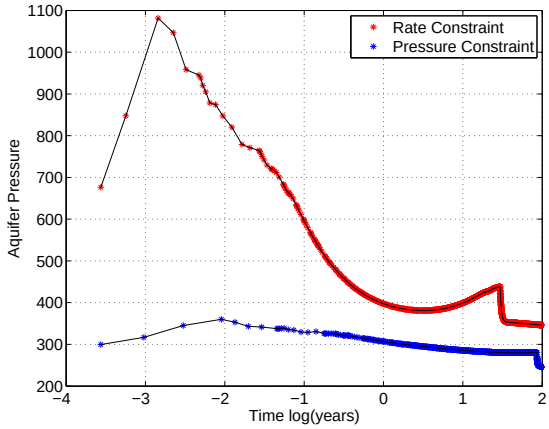

(b) Average aquifer pressure versus logarithm of time.

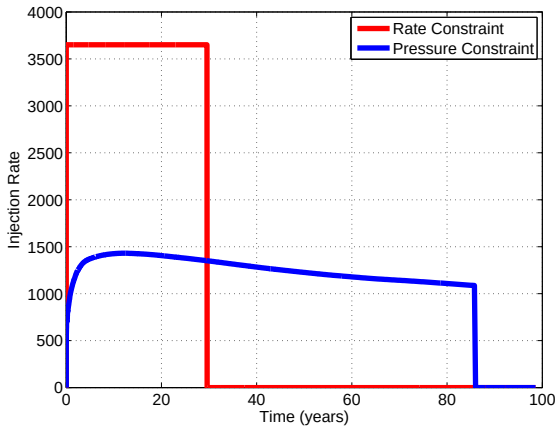

(c) Volumetric injection rate.

Figure 7: Aquifer and well pressure and injection rate in different injection scenarios shown for a test case.

Table 4: Simulation parameters used in the study.

Parameter	Description	Value
S_{rw}	Residual brine saturation	0.2
$S_{r_{CO_2}}$	Residual CO_2 saturation	0.2
$K_{r_{CO_2}}$	CO_2 relative permeability	$(1 - S_{CO_2} - S_{rw})^2$
K_{rw}	Brine relative permeability	$(S_w - S_{r_{CO_2}})^2$
ρ_{CO_2}	Supercritical CO_2 density at reference pressure	700.15 kg/m^3
ρ_w	Brine density at reference pressure	1033 kg/m^3
C_{rock}	Rock compressibility	0.3×10^{-6} 1/bar
C_{CO2}	CO_2 compressibility	0.375×10^{-4} 1/bar
C_{water}	Water compressibility	0.3×10^{-6} 1/bar
P_0	Reference pressure	400 bar
μ_{CO_2}	CO_2 viscosity	0.04 cP
μ_w	Brine viscosity	0.4 cP
q	Target injcetion rate	3600 m^3/day
P_{cr}	Critical well pressure	400 bar

4 Pressure analysis

We start by discussing the pressure responses for one particular realization. Then, we continue with the full analysis of all the 160 specified realizations made by combining the geological variable levels discussed earlier.

Some of the reported results are chosen at 2.4 hours (0.1 day), because at this time the maximum pressure value is calculated at the injection point compared to other times. In the start of injection, the injected CO_2 has to displace the water. In the start of injection, low CO_2 saturation around the injector causes low mobility for CO_2 and this results in a big pressure build-up (Figure 7).

Four types of responses are considered to compare the different simulation cases. One important question is how fast we can inject a fixed total volume into each realization. Pressure behavior in the system is studied by looking at the average aquifer pressure and the pressure elevation across the well. An overpressure region is defined in which the volumetric spread of over-pressurized locations in the model is measured. Finally, the farthest place from the injection point that a pressure build up has reached is reported for each realization to see the impact of heterogeneity and channels on how the pressure wave travels through the medium.

Figure 8 shows the pressure and saturation responses for the two injection scenarios for a selected simulation case. This realization has one lobe, parallel rock-type stratigraphy (i.e., low aggradation angle), up-dip progradation, high barrier coverage, and is faulted with open faults. The pressure buildup in Figures 8c and 8f tells how heterogeneity impacts the ability to maintain the pressure locally rather than transferring it across the medium. Comparing Figures 8b and 8c with Figures 8e and 8f, we see that imposing a pressure constraint significantly reduces the pressure buildup in the medium (as should be expected). However, the pressure disturbance propagates widely through the system in both cases (Figures 8c and 8f), far beyond the CO_2 invaded zones shown in Figures 8a and 8d.

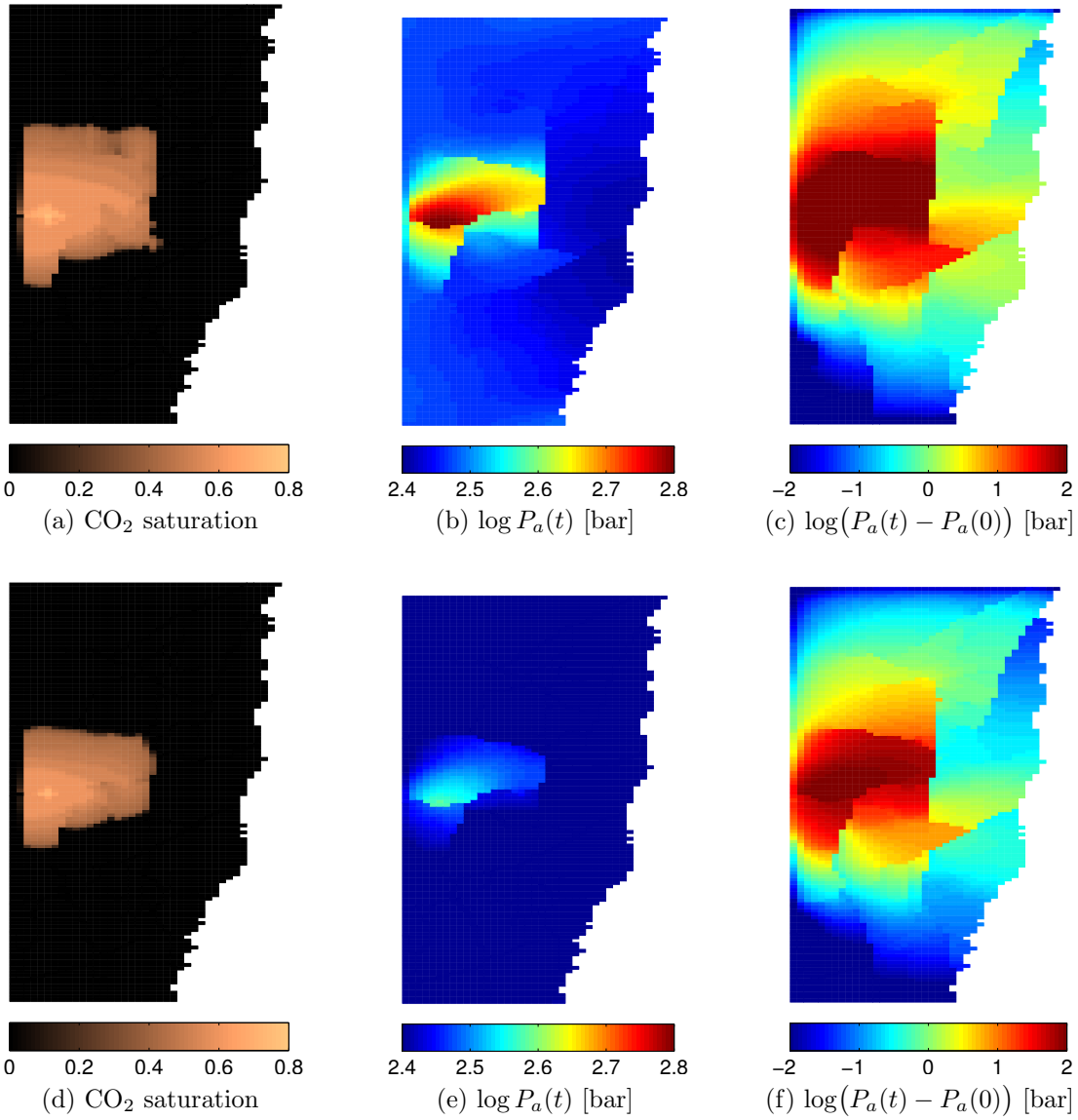

(a) CO_2 saturation (b) $\log P_a(t)$ [bar] (c) $\log\big(P_a(t) - P_a(0)\big)$ [bar]

(d) CO_2 saturation (e) $\log P_a(t)$ [bar] (f) $\log\big(P_a(t) - P_a(0)\big)$ [bar]

Figure 8: Top view of responses at the middle of the injection period (15 years). The first row corresponds to rate-constrained and the second row belongs to the pressure-constrained injection scenario.

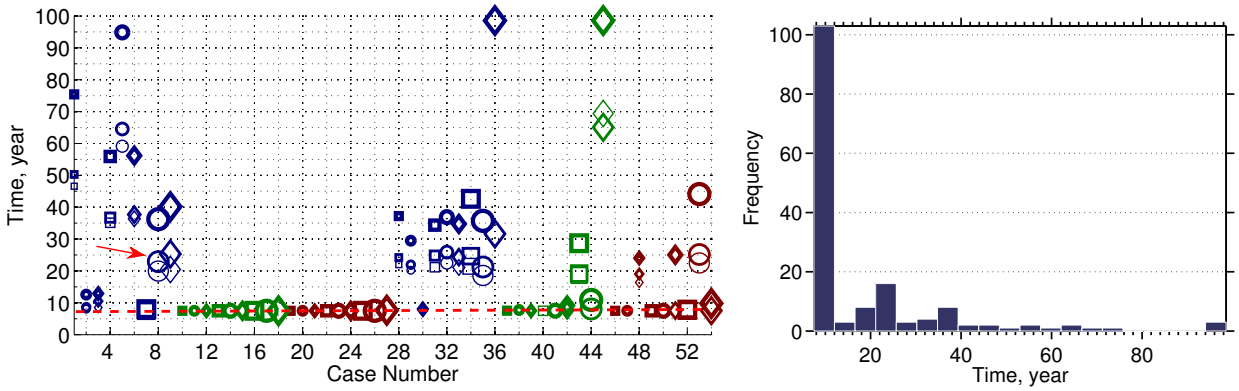

(a) Case plot of injection time in all cases.

(b) Histogram

Figure 9: Time to inject a quarter of the total specified CO_2 volume for all cases in the pressure-constrained scenario. The dashed red line in the left plot denotes the targeted injection time of 7.5 years, and the red arrow points to the case shown in Figure 8. (The case numbers refer to the different petrophysical realizations; in addition, each realization can have three different degrees of faulting. See Table 3.)

4.1 Injection time

In the pressure-constrained scenario, the lower the injectivity of the well is, the longer it will take to inject into the medium, if the pressure is to be kept below the critical limit. In some of the cases it takes longer than 100 years (i.e., longer than the total simulation time) to inject the specified CO_2 volume. To compare cases, we therefore calculate the time at which a quarter of the targeted volume is injected, which is less than 100 years for all simulation cases.

Figure 9 shows the injection time for all cases in the pressure-constrained scenario. For many cases, the injector keeps the target rate and thus completes the injection within the planned time period of 7.5 years (the dashed red line in the figure). The rest of the cases require longer injection time because of the lower injectivity of the medium. This leads to pressure control in the injector, followed by a decrease in the injection rate. In almost all the realizations with low aggradation angle, shown in blue color (Table 3), the injection rate is reduced below the constant target rate. Also cases with closed faults, denoted by thick markers, have (significantly) longer injection time. The effect of progradation direction is apparent in realizations with higher aggradation angle: for some of the cases colored green and red in the right half of the plot in Figure 9, injection takes longer than the corresponding cases in the left half. Therefore, down-dip progradation, independent of aggradation angle, can result in lower injectivity.

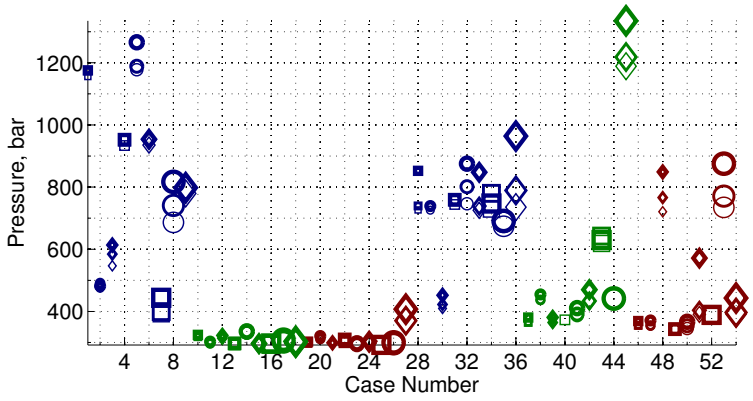

(a) Rate-constrained scenarios.

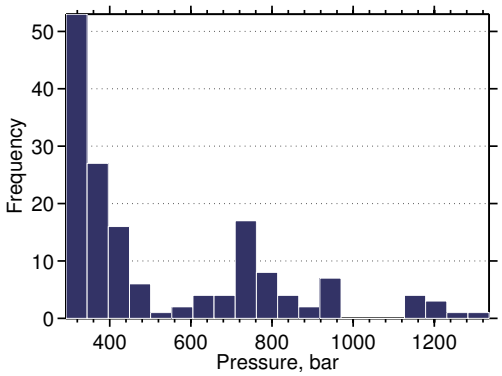

(b) Histogram, rate constrained.

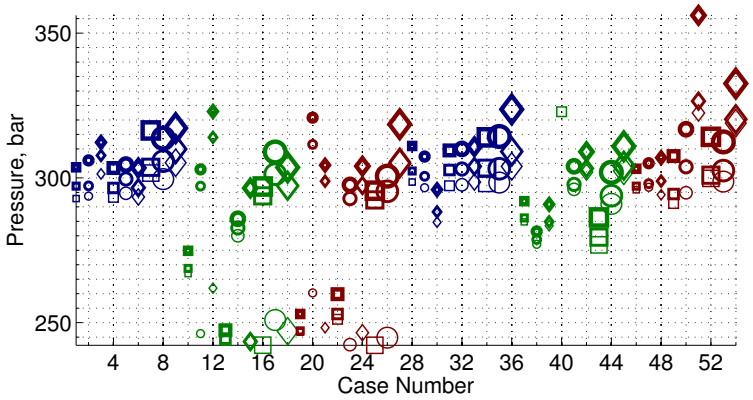

(c) Pressure-constrained scenarios.

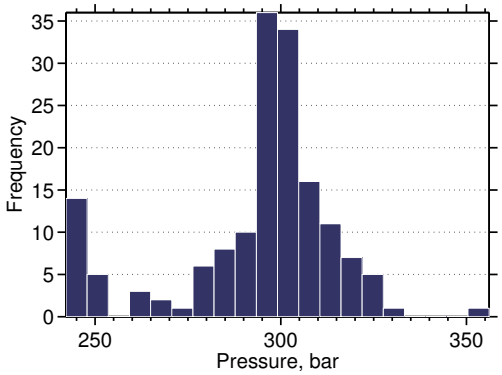

(d) Histogram, pressure constrained.

Figure 10: Average aquifer pressure values 2.4 hours after injection started. (The case numbers refer to the different petrophysical realizations; in addition, each realization can have three different degrees of faulting. See Table 3.)

4.2 Well and aquifer pressure

To see the overpressure caused by different heterogeneities, we compare cases for their average pressure and well pressure elevation. Average aquifer pressure 2.4 hours after the start of injection is plotted for all cases in Figures 10a and 10c; the corresponding histograms are shown in Figures 10b and 10d. In the rate-constrained scenario, high ranges of average pressure are observed (Figure 10a). Effects of aggradation angle, progradation and faulting are visible in the plot. Three clusters can be identified in the histogram of Figure 10b with medium, high and extreme pressure values. In Figure 10d, a small group of cases show lower pressures, while most of cases are distributed around the mean value ($\approx$ 300 bar).

We define the average elevation in the well pressure at time t_c as the temporal average of the difference between the bottom-hole pressure P_w and the average aquifer pressure $\bar{P}_a$:

$$\overline{\Delta P} = [\int_0^{t_c} (P_w - \bar{P}_a)\, \mathrm{d}t]/t_c. \tag{1}$$

The average well-pressure elevation is plotted for all cases in Figures 11a and 11c and histograms are shown in Figures 11b and 11d. Higher values imply a poor injectivity of the medium. For the rate-constrained scenarios, we see that maintaining the target rate will in many cases require a huge pressure elevation (up to 1400 bar in the worst cases) that would not be feasible nor possible to obtain. Pressure control on the injector reduces the range of pressure elevation variation below 170 bar.

Two regions can be identified in the medium, the region near the injection point; and the part of aquifer which is far from the injection point. The well-bore pressure is effected directly by heterogeneities in the near well-bore region, while the larger-scale region influences the average aquifer pressure. Pressure elevation variations in Figures 11a and 11b are influenced by the heterogeneity near the well-bore, where the reaction to injecting a fixed amount of CO_2 starts by a local pressure buildup. Heterogeneity on the scale of aquifer plays a considerable role in the range of variations in Figures 11c and 11d. In the pressure-constrained scenario, local pressure is controlled by putting a constraint on the well. Hence, the pressure elevation variations are controlled by the average aquifer pressure.

As we see in Figure 11a, low aggradation angle and down-dip progradation result in a poor injectivity and high pressure buildup in the injector. In particular, vertical transmissibility drops dramatically for low aggradation angles [2]. This restricts the pressure transfer within the injection layer, and therefore the pressure builds up locally around the well. Moreover, in cases with down-dip progradation the low permeability rocks surrounding river branches near the injector result in a local pressure buildup.

A group of cases in Figure 11c have a relatively low pressure elevation of less than 50 bar. These cases have a good injection quality, and the pressure is released through open boundaries easier than other cases. The rest of the cases show higher pressure elevation because of the heterogeneities in the larger scale, far from the injector. These results are obtained for a fixed injection location and one may observe different results, if one chooses to drill and complete the injector in the best formation with highest possible injectivity.

Faults influence both local pressure buildup near the injector as well as the average aquifer pressure. Therefore, they have a visible trend in many cases in Figures 11a and 11c (for example, see the three cases denoted by red circles in the right end of Figure 11a). This is specially more apparent in cases with high level of barriers.

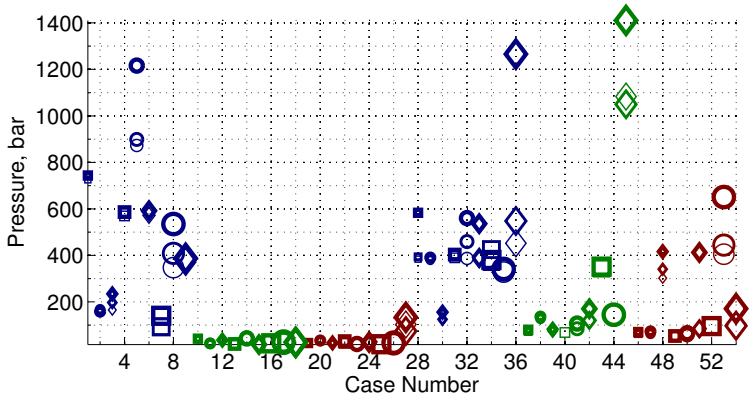

(a) Rate-constrained scenario.

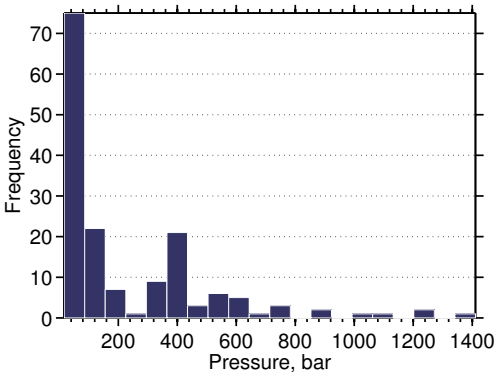

(b) Histogram, rate constrained.

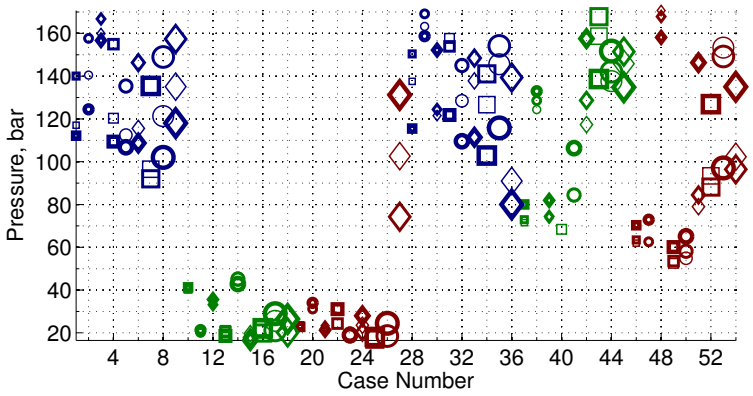

(c) Pressure-constrained scenarios.

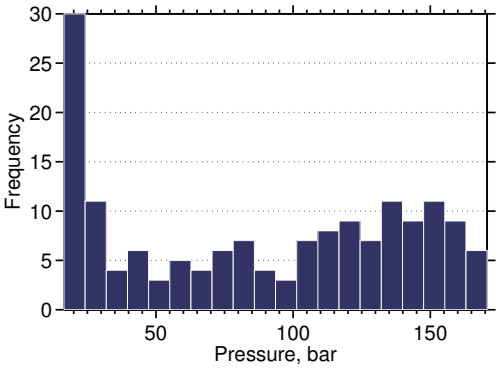

(d) Histogram, pressure constrained.

Figure 11: Average elevation in pressure for all cases after 2.4 hours. (The case numbers refer to the different petrophysical realizations; in addition, each realization can have three different degrees of faulting. See Table 3.)

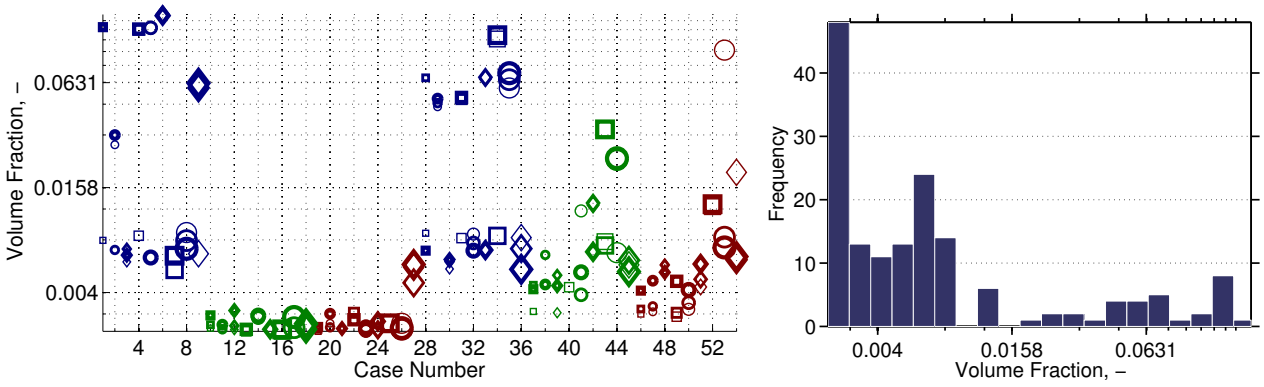

(a) Case plot of pressurized volume fractions.

(b) Histogram.

Figure 12: Pressurized volume fraction for all cases in the rate-constrained scenario. (The case numbers refer to the different petrophysical realizations; in addition, each realization can have three different degrees of faulting. See Table 3.)

4.3 Pressurized region

Here, we study the overpressure distribution in the medium defined so that all cells with a pressure higher than 300 bar value form a region that is called the pressurized region. Case plots and histogram of the ratio of pressurized volume to the total volume of all active cells in the model at the start of injection are given in Figure 12. Here, we clearly see that low aggradation angle is very influential in the pressure buildup in the injection zone. A group of cases with low aggradation angle have a relatively large pressurized region, but there are also a number of cases with low aggradation angles that have a relatively low pressurized fraction. In these cases, the medium is conductive toward the open boundaries and the heterogeneity in the medium does not cause a major pressure buildup. Other observation in Figure 12a is the progradation effect; down-dip progradation shows a rise in pressurized fraction for higher aggradation angles.

4.4 Buildup region

To study the pressure change, and how a pressure disturbance spreads through the medium, we use another metric. We calculate the pressure change by subtracting the initial hydrostatic pressure at each location from the current pressure. Different realizations are compared for the size of a region, which we call the buildup region, in which the pressure has increased from its initial value by 10 bar. The value of 10 bar was chosen to make sure that the region has not reached the boundaries in any of the studied cases. The smaller the buildup region is, the less volume will be exposed to pressure change in the aquifers (Figure 13).

Higher pressure in the medium will obviously cause a larger buildup region. Impact of progradation on the pressure buildup is illustrated in Figure 13a. Up-dip progradation shows a relatively lower pressure buildup compared to down-dip progradation cases. However, this effect is clearly overruled by aggradation, as cases with low aggradation angle show the same pressure buildup for both types of progradation directions (Note the blue colored markers that do not follow the lines in Figure 13a).

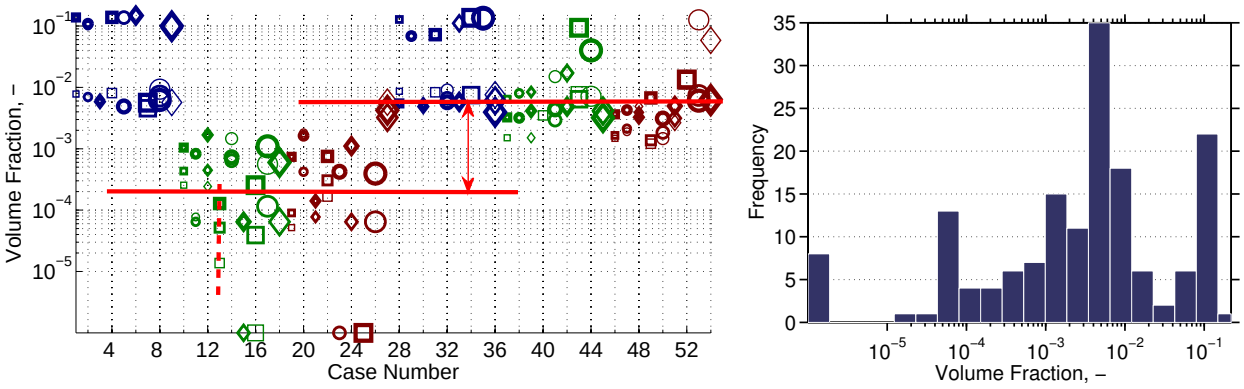

(a) Case plot of buildup volume fractions.

(b) Histogram.

Figure 13: Buildup volume fraction for all cases in the rate-constrained scenario. (The case numbers refer to the different petrophysical realizations; in addition, each realization can have three different degrees of faulting. See Table 3.)

Several cases in Figure 13a show a trend for the fault parameter. The dashed line shows the trend of buildup pressure increase due to fault feature variations in three cases. Faulting changes the geometry of layers and puts different layers adjacent to each other. This enhances the connectivity in the medium. Local heterogeneities and closed faults around the injector make a larger buildup region, because they cause higher pressure buildup in the domain. In these cases, the effect of heterogeneity of different scales, namely on the scale of near injector and far from injector, are combined causing a larger buildup fraction.

4.5 Farthest pulse

As discussed earlier, irregular geometries like faults and unconformities can lead to pressure spread in the domain. Looking at the volume fraction of pressurized and buildup regions helps in comparing cases for their pressure conductivity, but it does not show the extent of pressure spread in the medium. For that reason, we also look at the farthest cell from the injection point that falls within the buildup region defined earlier.

Figure 14 shows the farthest distance from the injector at which pressure buildup is observed for the different injection scenarios. In Figure 14b, three groups of cases can be identified: cases with zero distance of farthest pressure buildup pulse, cases with medium distances, and those with large distances from the injection point. Three specific cases are chosen as samples from each of the groups (see Figure 15 for example). In the first group (Figure 15a), the injector is placed in a permeable region and the medium is conductive toward open boundaries and hence the imposed injection pressure does not build up beyond the 10 bar threshold from its initial value, neither locally around the well nor globally in the aquifer scale. The cases in the second group (Figure 15b) have a medium range of 3–4 km of pressure-propagation distances from the injection point. Heterogeneity in these cases is not making a high pressure buildup around the injector and throughout the medium.

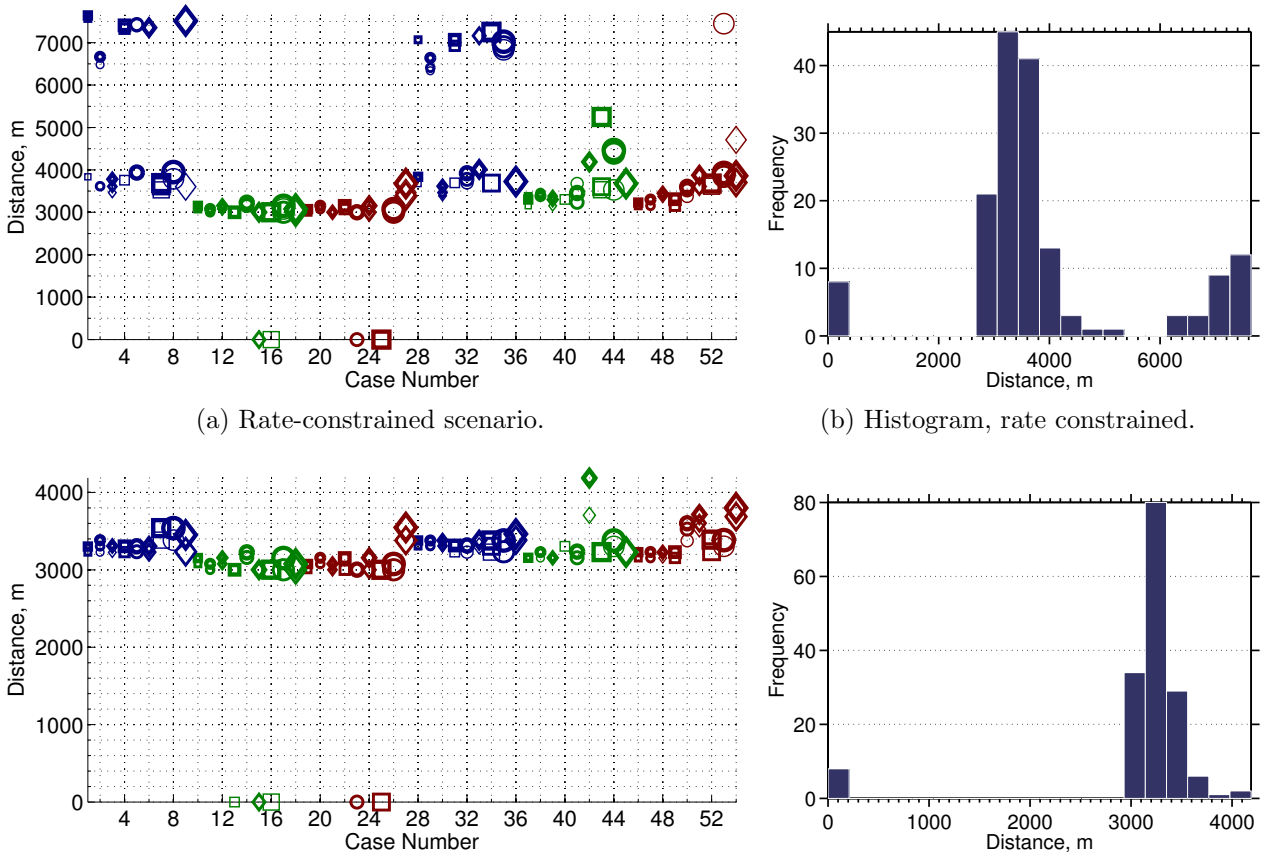

(a) Rate-constrained scenario.

(b) Histogram, rate constrained.

(c) Pressure-constrained scenario.

(d) Histogram, pressure constrained.

Figure 14: The farthest distance at which a pressure buildup is observed after 2.4 hours after injection start. (The case numbers refer to the different petrophysical realizations; in addition, each realization can have three different degrees of faulting. See Table 3.)

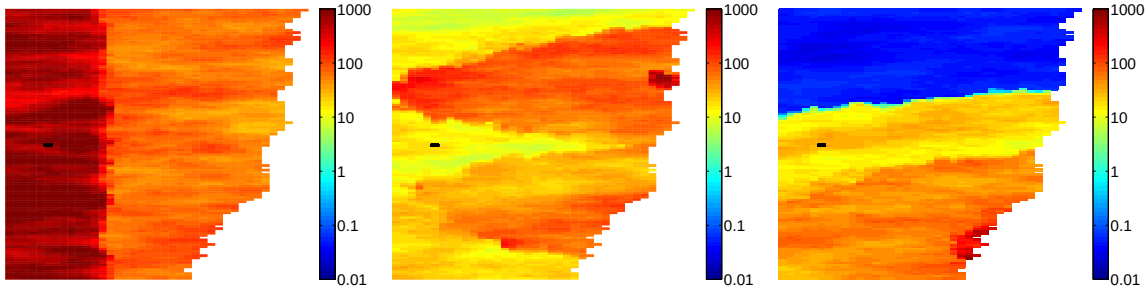

(a) (b) (c)

Figure 15: Top view of the permeability for three types of different realizations (in units milli Darcy); the well location is shown with black color in each plot. Heterogeneity can influence the pressure propagation within the medium. From case (a) to (c) the pressure build up shows higher values around the injector with larger propagation distances from the injection point.

In the third group (Figure 15c), low-permeable rocks in the injection layer cause a high pressure buildup around the injection point. If the injector zone is isolated by sealing heterogeneities, the pressure rises in a limited region. However, if the well is connected throughout the medium, and the heterogeneities in the aquifer scale contain relatively low permeability rocks, the pressure build up spreads wider in the aquifer. In Figure 15c, the injection point is located close to a low transmissibility rock. This rises the pressure level in the injector. Other parts of the aquifer are connected with poor quality rocks, resulting in a wide buildup region.

The farthest pulse distance ranges from 8 km to approximately 10 km in the extreme cases. By controlling the injection pressure, the maximum shrinks to slightly above 4 km (Figure 14d).

5 Discussion

So far, we reported the model responses that measure the pressure rise and pressure disturbance propagation in the domain. The pressurized volume fraction indicates the actual high pressures that may occur in an injection operation. The buildup volume fraction and the farthest pulse are indicators of how the pressure disturbance is spread in the system. We are interested in limiting both the pressure increase and the distance the elevated pressure propagates into the aquifer.

In most of the results, aggradation angle, progradation direction, and faults play a major role in the pressure behavior. For low aggradation angles, geological layers are made of rock types piled in a parallel stratigraphy. Thus, efficient vertical permeability is the harmonic average of these layers. If any of these layers contain a low-permeability rock, the vertical transmissibility will be low, and injecting into a limited space that is vertically sealed increases the pressure at the injection point.

The progradation direction can dominate the pressure behavior. It is very important to locate the injector in a high permeability zone that is connected to other parts of the domain via permeable channels. Injecting into the riverside of a shallow marine depositional system may result in locating the injection point in low-quality rocks between river branches joining the sea. This fact increases the pressure significantly near the injection point and can result in a high well-bore and aquifer pressure.

Structural deformations due to faulting process can increase the connectivity in the medium. If the overall transmissibility of the aquifer scale is high, the injection pressure releases through the open boundaries. However, if the injection area is surrounded by low-quality medium, the pressure increases in the aquifer and the connectivity enhanced by the fault geometries spreads the buildup region in the domain. On the other hand, sealing faults result in high pressures within closed zones around the injection point, but may also limit the propagation of the pressure disturbance in the domain.

From an operational perspective, pressure limits must be set to keep the operations within safe margins. One approach to study the safety of an operation could be setting critical limits on the pressure responses measured here. These limits should be inferred from realistic operational requirements and can then be used to filter out cases with undesirable/unacceptable pressure behavior. Herein, we assume that the limits are set to be 53 years for the injection

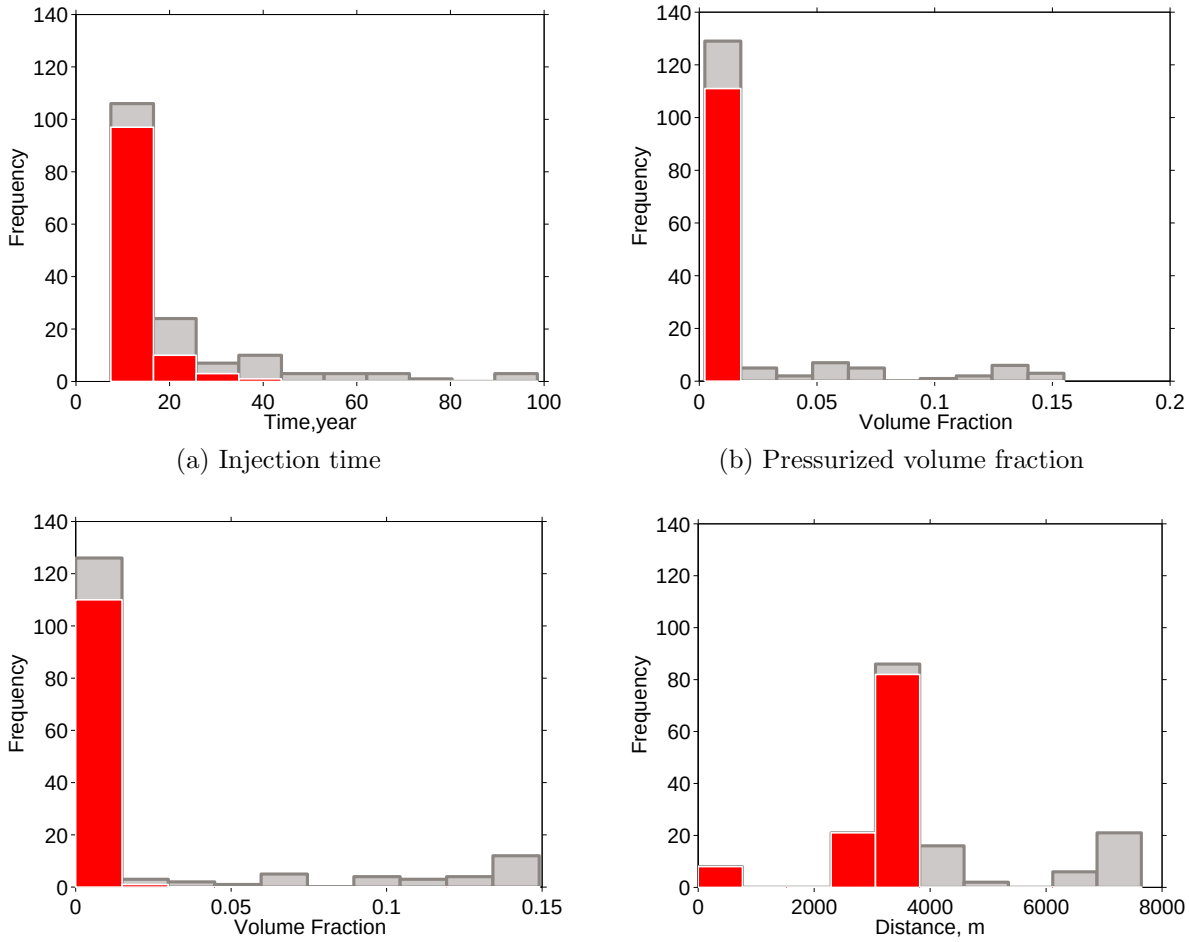

(a) Injection time

(b) Pressurized volume fraction

(c) Buildup volume fraction

(d) Farthest pulse propagation

Figure 16: Defined pressure criteria can be used to filter cases that are appropriate for the proposed injection scenario. Figure shows the histogram of filtered cases (red) compared with the histogram of all cases (gray) for different pressure responses.

time, 0.0787 for the pressurized volume fraction, 0.0745 for the buildup volume fraction, and 3822 m for the farthest pulse distance from the injection point. (These values are the mid-points of the range of variations in the results). By these assumptions, 49 cases out of the total number of 160 cases exceed the critical limits. Figure 16 shows the histogram of filtered cases compared with the histogram of all studied cases for each response.

6 Conclusions

This work is part of a comprehensive sensitivity study to assess the impact of geological heterogeneity on CO_2 injection and early plume migration. The aim of this study is to determine how different geological parameters impact the pressure buildup and establish which combinations that may potentially lead to buildup of high pressure values and large-distance propagation of elevated pressures. Simulation responses related to the pressure behavior in the system are defined and calculated for two CO_2 injection scenarios. Geological variations

in shallow-marine depositional systems are examined by using a large number of parametrized realizations representing a spectrum of sedimentological and structural scenarios.

The studied responses are most sensitive to aggradation, progradation direction, and faulting. Low aggradation angles inhibit the upward movement of the CO_2 plume and keep the flow restricted to the geological layers in which the CO_2 is injected. In cases with low rock quality in the injection layers, pressure will build up in the well-bore and large volumes may be forced down-dip and out through the lower boundary, as observed in [2]. In the down-dip progradation, the majority of the region around injection point is made of low quality rock and injecting in down-dip progradation normally ends up in a higher pressure buildup and a lower injectivity. Faults change the geometrical structure of the medium and they put different layers in contact. Pressure disturbances can leak through faults to larger distances from the injection point. Closed faults can significantly reduce the injectivity quality.

The workflow of the pressure study demonstrated here can be used in specific studies in the context of geological uncertainty. In particular, the insight of how different geological parameters impact the pressure buildup (and the migration of the CO_2 plume) can be used to predict optimal injection locations for this type of shallow-marine systems. The workflow can also be used for other depositional systems. However, since the study only involved two specific injection strategies, it is possible that one may obtain different outcomes than reported herein if significantly different values are used for the operational limits.

References

[1] M. Ashraf, K.-A. Lie, H. M. Nilsen, J. M. Nordbotten, and A. Skorstad. Impact of geological heterogeneity on early-stage CO_2 plume migration. In *CMWR*, 2010.

[2] M. Ashraf, K. A. Lie, H. M. Nilsen, and A. Skorstad. Impact of geological heterogeneity on early-stage CO_2 plume migration: Sensitivity analysis. In *ready for submission*, 2012.

[3] J. Birkholzer, Q. Zhou, J. Rutqvist, P. Jordan, K. Zhang, and C.-F. Tsang. Research project on co2 geological storage and groundwater resources: Large-scale hydrological evaluation and modeling of impact on groundwater systems. Technical report, Lawrence Berkeley National Laboratory, Berkeley, CA, USA, 2008.

[4] B. Cailly, P. Le Thiez, P. Egermann, A. Audibert, S. Vidal-Gilbert, and X. Longaygue. Geological storage of CO_2: A state-of-the-art of injection processes and technologies. *Oil & Gas Science and Technology*, 60(3):517–525, 2005.

[5] A. Cavanagh and N. Wildgust. Pressurization and brine displacement issues for deep saline formation CO_2 storage. *Energy Procedia*, 4:4814–4821, 2011.

[6] E. R. Chabora and S. M. Benson. Brine displacement and leakage detection using pressure measurements in aquifers overlying co_2 storage reservoirs. *Energy Procedia*, 1(1):2405–2412, 2009.

[7] J. A. Howell, A. Skorstad, A. MacDonald, A. Fordham, S. Flint, B. Fjellvoll, and T. Manzocchi. Sedimentological parameterization of shallow-marine reservoirs. *Petroleum Geoscience*, 14(1):17–34, 2008.

[8] T. Le Guenan and J. Rohmer. Corrective measures based on pressure control strategies for CO_2 geological storage in deep aquifers. *International Journal of Greenhouse Gas Control*, 2010.

[9] T. Manzocchi, J. N. Carter, A. Skorstad, B. Fjellvoll, K. D. Stephen, J. A. Howell, J. D. Matthews, J. J. Walsh, M. Nepveu, C. Bos, et al. Sensitivity of the impact of geological uncertainty on production from faulted and unfaulted shallow-marine oil reservoirs: objectives and methods. *Petroleum Geoscience*, 14(1):3–11, 2008.

[10] J. D. Matthews, J. N. Carter, K. D. Stephen, R. W. Zimmerman, A. Skorstad, T. Manzocchi, and J. A. Howell. Assessing the effect of geological uncertainty on recovery estimates in shallow-marine reservoirs: the application of reservoir engineering to the SAIGUP project. *Petroleum Geoscience*, 14(1):35–44, 2008.

[11] S. P. Neuman and P. A. Witherspoon. Theory of flow in a confined two aquifer system. *Water Resources Research*, 5(4):803–816, 1969.

[12] J. Nicot. Evaluation of large-scale CO_2 storage on fresh-water sections of aquifers: an example from the Texas Gulf Coast Basin. *International Journal of Greenhouse Gas Control*, 2(4):582–593, 2008.

[13] J. Rutqvist, J. Birkholzer, F. Cappa, and C.-F. Tsang. Estimating maximum sustainable injection pressure during geological sequestration of CO_2 using coupled fluid flow and geomechanical fault-slip analysis. *Energy Conversion and Management*, 48(6):1798–1807, 2007.

[14] J. Rutqvist and C. F. Tsang. A study of caprock hydromechanical changes associated with CO_2 injection into a brine formation. *Environmental Geology*, 42:296–305, 2002. 10.1007/s00254-001-0499-2.

[15] Schlumberger. Eclipse technical description manual, 2009.

[16] S. Solomon, D. Qin, M. Manning, Z. Chen, M. Marquis, K. B. Averyt, M. Tignor, and H. L. Miller, editors. *Climate Change 2007 – The Physical Science Basis: Working Group I Contribution to the Fourth Assessment Report of the IPCC*. Cambridge University Press, Cambridge, UK and New York, NY, USA, Sept. 2007.

[17] L. G. H. van der Meer. Investigations regarding the storage of carbon dioxide in aquifers in the Netherlands. *Energy Conversion and Management*, 33(5-8):611–618, 1992.

[18] L. G. H. van der Meer. The conditions limiting CO_2 storage in aquifers. *Energy Conversion and Management*, 34(9-11):959–966, 1993.